Proc. Natl. Acad. Sci. USA
Vol. 95, pp. 5495–5500, May 1998
Biochemistry

Snapshot of a phosphorylated substrate intermediate by kinetic crystallography

HELENA KÄCK*, KATHARINE J. GIBSON†, YLVA LINDQVIST*‡, AND GUNTER SCHNEIDER*‡

*Molecular Structural Biology, Department of Medical Biochemistry and Biophysics, Karolinska Institutet, 171 77 Stockholm, Sweden; and †DuPont Central Research and Development, Experimental Station, P. O. Box 80328, Wilmington DE 19880-0328

Communicated by George H. Lorimer, Department of Chemistry and Biochemistry, University of Maryland, College Park, MD, February 26, 1998 (received for review November 3, 1997)

ABSTRACT **The ATP-dependent enzyme dethiobiotin synthetase from *Escherichia coli* catalyses the formation of dethiobiotin from CO_2 and 7,8-diaminopelargonic acid. The reaction is initiated by the formation of a carbamate and proceeds through a phosphorylated intermediate, a mixed carbamic phosphoric anhydride. Here, we report the crystal structures at 1.9- and 1.6-Å resolution, respectively, of the enzyme–MgATP–diaminopelargonic acid and enzyme–MgADP–carbamic–phosphoric acid anhydride complexes, observed by using kinetic crystallography. Reaction initiation by addition of either $NaHCO_3$ or diaminopelargonic acid to crystals already containing cosubstrates resulted in the accumulation of the phosphorylated intermediate at the active site. The phosphoryl transfer step shows inversion of the configuration at the phosphorus atom, consistent with an in-line attack by the carbamate oxygen onto the phosphorus atom of ATP. A key feature in the structure of the complex of the enzyme with the reaction intermediate is two magnesium ions, bridging the phosphates at the cleavage site. These magnesium ions compensate the negative charges at both phosphate groups after phosphoryl transfer and contribute to the stabilization of the reaction intermediate.**

A catalytic strategy used by many enzymes is to use nucleotide triphosphates, in particular ATP, for leaving group activation. In general, this strategy can be accomplished by transfer of the γ-phosphoryl group of the nucleotide to the substrate. The resulting phosphorylated intermediate decomposes into phosphate and product. The penultimate enzyme in the biotin biosynthetic pathway, dethiobiotin synthetase (DTBS), uses this strategy. This enzyme catalyzes the ATP-dependent formation of the cyclic urea dethiobiotin from (7*R*,8*S*)-diaminononanoic acid [7,8-diaminopelargonic acid (DAPA)] and CO_2. As a catalyst, the enzyme is rather inefficient, with $k_{cat} = 1.5\ min^{-1}$ under standard assay conditions (2, 4). DTBS was first studied by Eisenberg (1, 2), who proposed that the reaction consists of several steps (Fig. 1). The first step, formation of a DAPA carbamate, later was shown to proceed regiospecifically at N7 (3–5). The second proposed intermediate, a mixed carbamic–phosphoric acid anhydride formed by transfer of the γ-phosphoryl group of ATP to a carbamate oxygen (6), has been isolated, with a lifetime of ≈25 min under certain conditions (7). It has been suggested that the last step, ring closure, proceeds through a tetrahedral intermediate (3).

The three-dimensional structure of the enzyme (5, 8, 9) revealed a homodimer with the two equivalent active sites, separated by ≈25 Å, at the interface between the two subunits. The structure of DTBS is similar to the structure of other phosphotransferases, in particular adenylate kinase (10) and p21ras (11). Crystallographic studies (3) of complexes of DTBS with DAPA and/or a nonhydrolyzable ATP analogue, adenylyl [β,γ-methylene]diphosphonate (AMPPCP), suggested that conformational changes during catalysis were minor and that these crystals might be suitable for time-resolved crystallography.

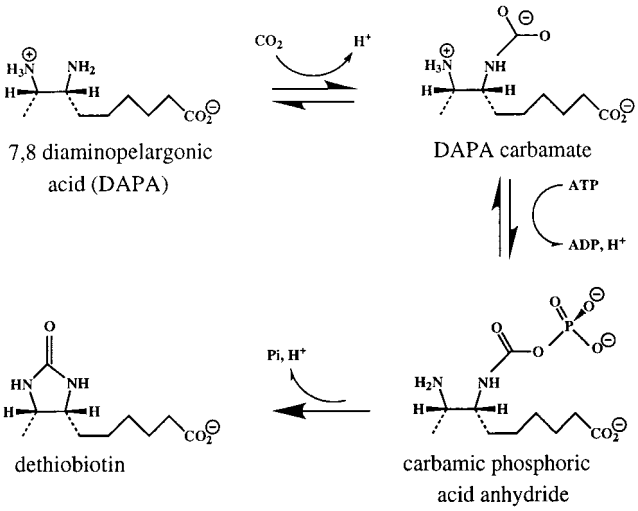

FIG. 1. Reaction scheme for dethiobiotin synthetase.

Recently, the crystal structures of several phosphoenzyme intermediates have been determined. In these cases [alkaline phosphatase (12), fructose-2,6-bisphosphatase (13), and nucleoside diphosphate kinase (14)], a histidine side chain is phosphorylated during the catalytic reaction. Here, we report the structure of the complex of DTBS with the mixed carbamic phosphoric acid anhydride intermediate, the first crystal structure of a substrate-derived phosphorylated reaction intermediate trapped during the catalytic reaction. The structure provides insights into how enzymes might stabilize such intermediates.

MATERIALS AND METHODS

Crystallization and Catalytic Activity in the Crystal. DTBS was expressed and purified as described (4, 8). Crystallization was done by using vapor diffusion. The reservoir solution

Abbreviations: DTBS, dethiobiotin synthetase; DAPA, 7,8-diaminopelargonic acid.

Data deposition: The atomic coordinates have been deposited in the Protein Data Bank, Biology Department, Brookhaven National Laboratory, Upton, NY 11973 [reference 1a82 for the enzyme–ATP–Mg(II)–substrate complex and 1dak for the enzyme–ATP–$Mg(II)_2$–intermediate complex].

‡To whom reprint requests should be addressed. e-mail: gunter@alfa.mbb.ki.se or ylva@alfa.mbb.ki.se.

The publication costs of this article were defrayed in part by page charge payment. This article must therefore be hereby marked "*advertisement*" in accordance with 18 U.S.C. §1734 solely to indicate this fact.

Table 1. Details of data collection and refinement

	100 mM Mg^{2+}		5 mM Mg^{2+}
	t = 0 s	t = 80 s	
Spacegroup	C2	C2	C2
Cell dimensions			
a, b, c, Å	72.9, 47.9, 60.9	72.7, 47.9, 60.7	72.7, 48.2, 61.1
β, °	106.5	106.5	106.6
Resolution, Å	1.8–20	1.9–20	1.6–20
Highest resolution shell	(1.8–1.86)	(1.9–1.97)	(1.6–1.66)
Reflections, n			
Total	47,020	49,544	84,867
Unique	18,671	15,510	26,601
Completeness, %	98.7 (93.5)	98.4 (88.4)	99.1 (92.4)
R_{merge}	3.0 (11.6)	4.0 (5.8)	7.8 (43.6)
I/σ	25.6 (7)	28.6 (14)	16.1 (2.8)
$R_{refinement}$, %	19.0	17.9	18.4
R_{free}, %	24.6	21.3	21.1
B factor, $Å^2$			
Protein atoms	10.8	10.1	12.2
Nucleotide	13.2	12.7	15.1
Substrate/intermediate	11.8	12.1	13.8
Root-mean-square deviation			
Bond distance, Å	0.010	0.009	0.006
Bond angle, °	1.67	1.78	1.3

contained 100 mM buffer at pH 6.5, 100 mM MgAc, and 9–12% polyethylene glycol 8000. Crystals that belong to space group C2 grew within a few days from hanging drops prepared by mixing 7 μl of the reservoir solution with 3 μl of protein (30 mg/ml). Crystals, previously incubated in 5 mM ATP for 1 h, were crosslinked with a 2–3% glutaraldehyde solution. The reaction was interrupted after 1–2 s by addition of 1/5 volume of 1 M glycine, and crystals were washed extensively to remove excess reagents. Activity measurements of DTBS crystals were carried out by using a carbon dioxide fixation assay similar to one previously described (4). Crosslinked crystals were transferred to 20 μl of buffer solution containing 0.1 M Mops at pH 7.5, 0.1 M MgAc, and 1.5 mM ATP. The reaction was started by addition of 10 μl of substrate solution containing 12 mM [^{14}C]$NaHCO_3$, 0.3 mM EDTA, 0.1 M Mops pH 7, and 1.5 mM DAPA; 5-μl aliquots were quenched in 10% acetic acid at defined times and taken to dryness on a hotplate to remove unreacted [^{14}C]CO_2. The residue was dissolved with a small volume of water, and ^{14}C radioactivity was detected by scintillation counting. As a control, crystals were left for 2 h in 30 μl of the buffer solution, and the supernatant was assayed for catalytic activity.

Reaction Initiation and Crystallographic Data Collection. The phosphorylated reaction intermediate was trapped in the crystals by two procedures. In the first approach (experiment A), noncrosslinked crystals of DTBS, either grown under CO_2-free conditions or incubated in a CO_2-free mother liquor at pH 6.5, were incubated in 5 mM ATP, 15 mM DAPA, 18% polyethylene glycol 8000, 100 mM MgAc, and 20% 2-methyl-2,4-pentanediol for 1 h. 2-Methyl-2,4-pentanediol was included as cryoprotectant. One crystal was mounted in a cryo stream at 100 K for data collection (t = 0 s, DTBS–MgATP–DAPA complex). The catalytic reaction was started by the addition of 30 mM $NaHCO_3$. At various time intervals, crystals were mounted in the cryo stream and complete x-ray data sets were obtained. In the second approach (experiment B), crystals were equilibrated with 5 mM ATP and 5 mM MgAc at pH 6.5 for 1 h at room temperature. The crystals were then transferred to a solution containing 15 mM DAPA, 30 mM $NaHCO_3$, 0.5 mM EDTA, 5 mM ATP, 5 mM MgAc, 18% polyethylene glycol 8000, and 20% 2-methyl-2,4-pentanediol at pH 6.5 and left in 4°C for 1 h before cryofreezing in a nitrogen stream. Data were collected at a Rikagu rotating anode by using a MAR image plate detector (MAR Research, Hamburg) and at beamline ID 9 at the ESRF (Grenoble, France) by using a charge-coupled device detector. X-ray data were processed with DENZO and SCALEPACK (15) (Table 1).

Crystallographic Model Building and Refinement. Initial phases were obtained from a refined structure of DTBS in complex with ADP and DAPA (3), and the substrate, product, and active site solvent molecules were excluded from the structure factor calculation. The substrates and the reaction intermediate were clearly visible in the electron density maps and were modeled by using O (16). Alternatively, the difference electron density obtained from the t = 80 s data was modeled and refined as a mixture of carbamylated DAPA and a phosphate ion, with van der Waals repulsion turned off. Crystallographic refinement was performed with XPLOR (17) and REFMAC (18). One typical round of refinement consisted of several cycles of positional refinement, followed by model building (mostly adding/deleting water molecules). At the end, individual B-factor refinement was carried out. In the last

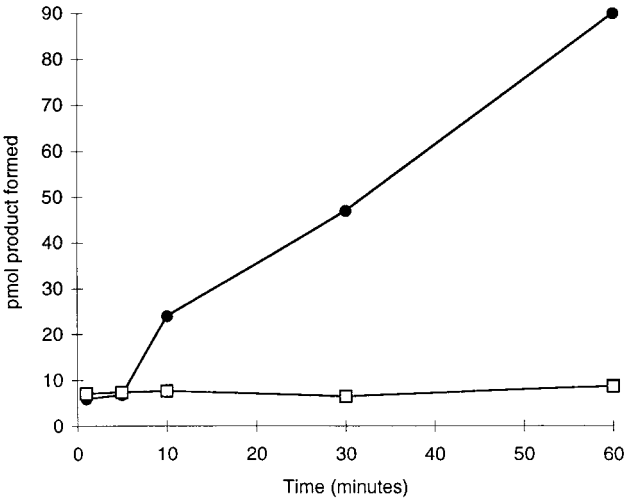

FIG. 2. Catalytic activity in DTBS crystals. Circles, catalytic activity in the presence of crosslinked crystals of DTBS; squares, catalytic activity in the supernatant after incubation with crosslinked crystals.

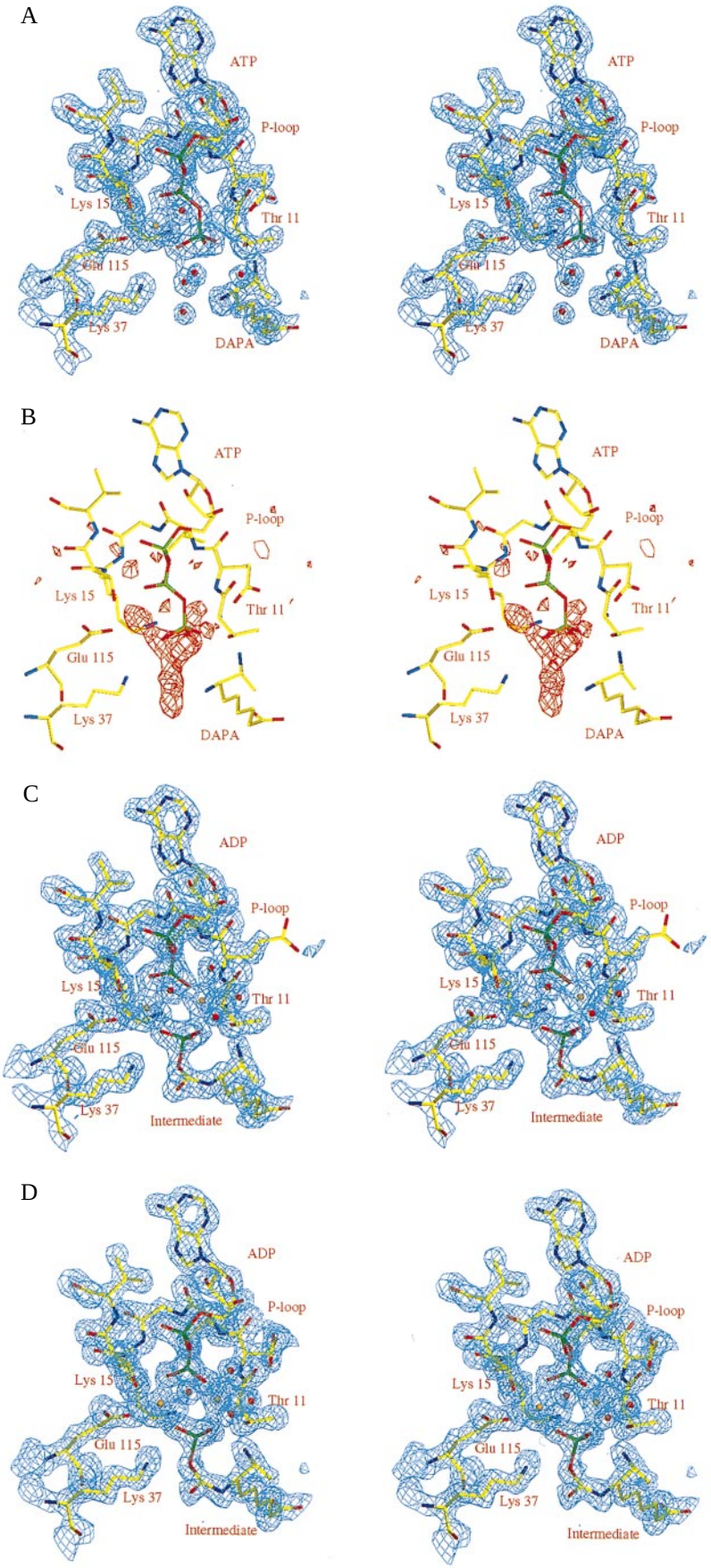

FIG. 3. (*A*) Stereo view of the refined 2Fo-Fc electron density map (contoured at 1.2σ) at the active site of the DTBS–MgATP–DAPA complex (t = 0). The structural model of the refined complex is superposed. (*B*) Stereo view of a $F_o - F_c$ electron density map (contoured at 3σ), covering the same part of the active site, calculated with data collected 80 s after reaction initiation (experiment A). The electron density map was calculated with phases from the DTBS–MgATP–DAPA complex, excluding active site solvent molecules, the γ-phosphate, and the metal ion from the structure factor calculation. The structure of the DTBS–MgATP–DAPA complex is superimposed. (*C*) Stereo view of the refined $2F_o - F_c$ electron density map (contoured at 1.2σ) for the DTBS–MgADP–intermediate (t = 80 s) complex, same view as above (experiment A). A model of the refined DTBS–MgADP–carbamic–phosphoric acid anhydride complex is included. (*D*) Stereo view of the refined $2F_o - F_c$ electron density map (contoured at 1.2σ) for the DTBS–MgADP–intermediate complex, obtained from experiment B. A model of the refined DTBS–MgADP–carbamic–phosphoric acid anhydride complex is included. Golden spheres indicate magnesium ions, and red spheres indicate solvent molecules

cycle, the occupancies of the substrates, ADP, and the intermediate were refined (ADP 0.97, carbamic phosphoric anhydride 0.94). Details of refinement and models are given in Table 1.

RESULTS AND DISCUSSION

Catalytic Activity in the Crystal. A prerequisite for time-resolved crystallography is that catalytic activity can be obtained in the crystalline state. Crystals of DTBS proved catalytically active, even after glutaraldehyde crosslinking (Fig. 2). No activity was released into the supernatant above such crystals after 2 h of incubation in buffer without precipitant. This result shows that the observed activity was caused by crystalline enzyme not by enzyme molecules dissolved from the crystal surface. The amount of product formed after 1 hour corresponded to >1 mol/mol subunit of the enzyme and probably represents multiple turnovers by DTBS molecules deep enough in the crystals to have escaped glutaraldehyde inactivation.

Trapping of the Intermediate in the Crystal. Two different strategies were used to trap the phosphorylated reaction intermediate. The first approach was to prepare crystals of the complex of DTBS–MgATP–DAPA under CO_2-free conditions. This complex corresponds to the reaction time $t = 0$ s. The catalytic reaction was then initiated at 20°C by soaking $NaHCO_3$ into the crystals, and at various time intervals the reaction was stopped by flash-freezing in a cryo stream at 100 K (19). The second approach takes advantage of the relative stability of the phosphorylated reaction intermediate at lower temperatures (7). Crystals preincubated in ATP at low Mg^{2+} concentration (5 mM) were soaked in solution containing substrates for ≈60 min at 4°C before cryogenic data collection. Both methods were successful in capturing the phosphorylated reaction intermediate, and the resulting difference electron density maps show the same features despite the difference in Mg^{2+} concentration.

The electron density maps calculated from data collected before the addition of carbon dioxide ($t = 0$ s) show well defined electron density for MgATP and DAPA (Fig. 3*a*). DAPA is bound with the diamino group pointing toward the γ-phosphate of ATP, and the carboxyl end interacts with residues from the second subunit, much as in the DTBS–DAPA–N7–carbamate binary complex (3, 5). As expected, no electron density consistent with carbamylation of N7 was observed. Instead, the N7 amino group forms hydrogen bonds with the side chain of Ser41 and a water molecule. The N8 amino group interacts with a solvent molecule and one of the oxygen atoms of the γ-phosphate.

The pattern of hydrogen bonds between the enzyme and ATP (Fig. 4*a*) is, with a few exceptions, identical to that described for the interaction of DTBS with the ATP analogue AMPPCP (3). One important exception is the hydrogen bonds formed by the main chain amide of Glu12 and a solvent molecule to the β,γ-bridge oxygen atom of ATP, which were not observed in the complex with AMPPCP where this oxygen is replaced by a carbon atom. The triphosphate is bound through an intricate network of hydrogen bonds, mainly from main chain amide groups of residues in the phosphate binding loop, as in other nucleotide binding proteins (10, 11). Two conserved lysine residues, Lys-15 and Lys-37, form hydrogen bonds to oxygen atoms of the β and γ phosphates, respectively. The ATP molecule is anchored further to the enzyme through a magnesium ion (site I). Oxygen atoms from the β- and γ-phosphate groups of ATP, the side chains of Asp-54, Thr-16, and Glu-115, and a water molecule are coordinated to this metal ion in an octahedral geometry. This metal binding site also is found in other ATP- and GTP-binding phosphotransferases (10, 11), and its roles in catalysis are manifold. It positions the γ-phosphate group relative to the attacking nucleophile, stabilizes the negative charge on the phosphate oxygen atoms, thereby facilitating nucleophilic attack, maintains ADP as a good leaving group, and stabilizes the transition state during phosphoryl transfer (20–22).

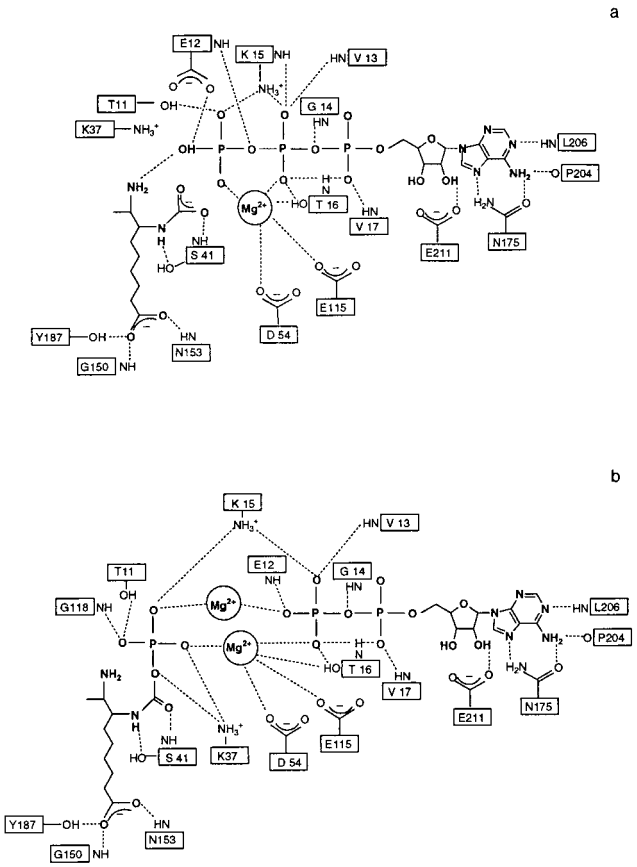

FIG. 4. Polar interactions of the substrate (*a*) and the reaction intermediate (*b*) with protein atoms at the active site of DTBS. Hydrogen bonds (cutoff distance 3.2 Å) are shown with dotted lines. Coordination bonds from atoms of the protein and the substrate/reaction intermediate to the Mg^{2+} ions are included.

Initiation of the reaction by the addition of CO_2 to the DTBS–MgATP–DAPA crystals requires the formation of the carbamylated DAPA before phosphoryl transfer can occur. The structure of the binary complex of DTBS with the N7–carbamate of DAPA has been determined (3). When this structure is compared with the structure of the CO_2-free DTBS–MgATP–DAPA complex (based on their Cα coordinates), the two DAPA molecules superpose well. The superposition suggests that the carbamate group would bridge the space between the N7 nitrogen atom of DAPA and the γ-phosphate of ATP and that one carbamate oxygen would be 3.7 Å away from the phosphorus atom. This oxygen atom would be almost perfectly aligned for an in-line nucleophilic attack on the γ-phosphorus atom (Fig. 5).

In difference electron density maps calculated from data collected 80 s after reaction initiation by the addition of bicarbonate to crystals of DTBS–MgATP–DAPA or, alternatively, from data collected on crystals incubated with substrates at low temperature, there is strong positive difference electron density extending from the N7 amino group of DAPA toward the nucleotide, consistent with the formation of the phosphorylated reaction intermediate (Fig. 3 *b–d*). No electron density was observed at the position expected for the γ-phosphate of ATP, indicating that the nucleotide was bound as ADP. The mixed carbamic–phosphoric acid anhydride and ADP accumulate in the crystals as the major species, as judged from occupancies (>0.9) and B-factors (comparable to those of protein atoms) (Table 1). In a control experiment, the density also was modeled and refined as a carbamylated DAPA and a phosphate ion. This resulted in similar occupancies and identical bond distances between the phosphorus atom

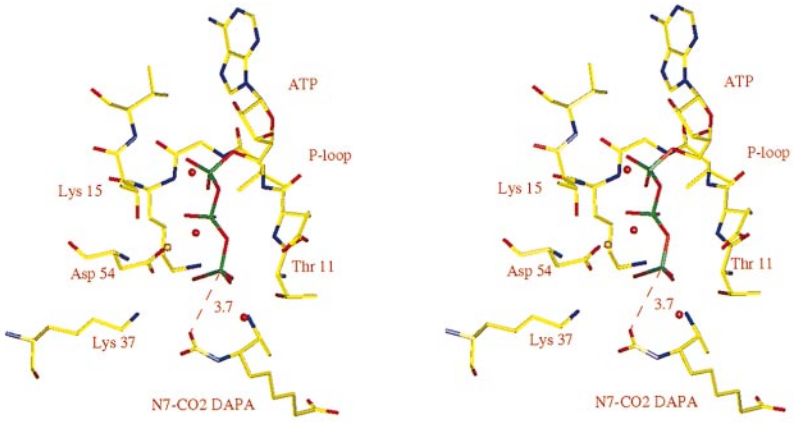

FIG. 5. Proposed structure of the complex of DTBS–MgATP–DAPA carbamate. The figure was composed from the structures of the DTBS–MgATP–DAPA ternary complex ($t = 0$ s) and the binary complex of DTBS with carbamylated DAPA (3). The structure is consistent with an in-line attack of a carbamate oxygen atom on the γ-phosphorus atom of ATP. Golden spheres indicate magnesium ions, and red spheres indicate solvent molecules.

and one of the carbamate oxygens (1.8 Å). Such a structural arrangement thus would require overlap of a phosphate oxygen and a carbamate oxygen, which is physically impossible.

One of the carbamate oxygens is within hydrogen bonding distance of the side chain of Lys-37. A crucial role of this residue in catalysis and substrate binding had been suggested by mutagenesis studies (23). The phosphoryl oxygens of the mixed carbamic–phosphoric acid anhydride intermediate interact through hydrogen bonds with main chain amides of Gly-118 and the side chains of Lys-15, Thr-11, Lys-37, and Glu-115, in addition to the site I Mg^{2+} ion (Fig. 4*b*). The DAPA moiety of the anhydride shows the same hydrogen bond pattern as in the DTBS–MgATP–DAPA complex.

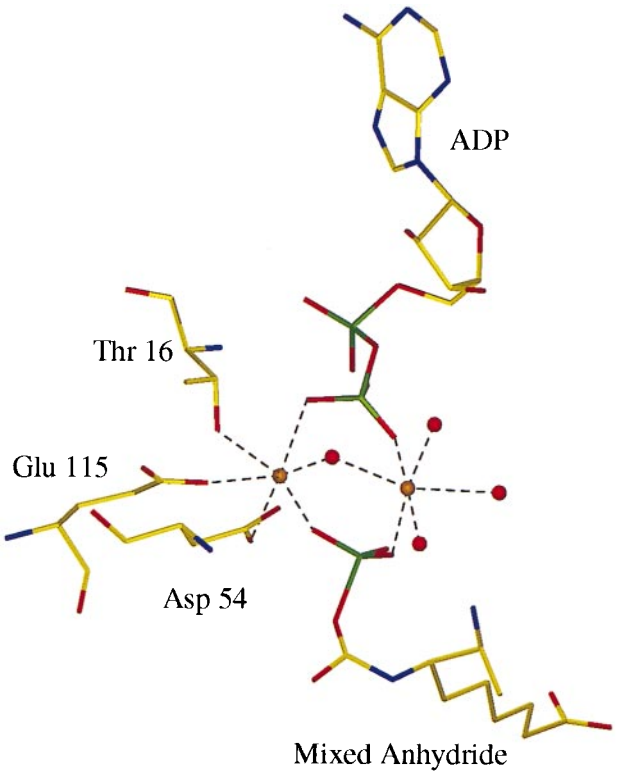

FIG. 6. Refined structure of the metal sites of the complex of DTBS with ADP and a reaction intermediate, the mixed carbamic–phosphoric acid anhydride. Golden spheres indicate magnesium ions, and red spheres indicate solvent molecules. Coordination bonds are shown by dotted lines.

Superposition of the DTBS structures before and after phosphoryl transfer shows that the transferred phosphoryl group has moved ≈1.4 Å from its position in the ATP complex to the one observed in the complex with the intermediate. The comparison implies that the reaction proceeds with inversion of the configuration at the phosphorus atom.

A surprising feature in this complex is a second Mg^{2+} binding site located on the opposite side of the nucleotide from metal site I, facing bulk solvent (Fig. 6). This Mg^{2+} ion is bound to one oxygen atom of the β-phosphate of ADP and to one oxygen atom of the phosphate of the mixed anhydride. However, the ion is not bound to the protein in any way. Instead, four solvent molecules complete the almost perfect octahedral coordination sphere. Thus, although only one metal ion was observed in the DTBS–MgAMPPCP–DAPA–CO_2 (3) and DTBS–MgATP–DAPA complexes, two metal ions interact with the β-phosphate of ADP and the phosphate of the mixed anhydride after phosphoryl transfer has occurred. These metal ions bound at the phosphate cleavage site might stabilize the DTBS–mixed anhydride–ADP complex. The experiments at moderate concentration of Mg^{2+} suggest that the observed structure of the phosphorylated intermediate is relevant to catalysis under physiological conditions. The engagement of two metal ions in phosphoryl transfer reactions is not without precedent. For instance, phospho*enol*pyruvate carboxykinase (24), pyruvate kinase (25), and glutamine synthetase (26) each require two divalent cations for activity, although the precise function of these metal ions in the catalytic reaction differs among these enzymes.

In conclusion, kinetic crystallography has provided direct evidence for the existence of a phosphorylated reaction intermediate during catalysis at the active site of dethiobiotin synthetase. This study reveals one mechanism for how enzymes stabilize such phosphorylated reaction intermediates and thus provides insights into the structural basis of ATP-mediated leaving group activation in enzymes.

We thank the ESRF (Grenoble, France) for access to synchrotron radiation and in particular D. Bourgeois and M. Wulff for generous help at beamline ID 09. This work was supported by grants from the Swedish Natural Science Research Council, the Foundation for Strategic Research, and the Swedish Agricultural Research Council.

1. Eisenberg, M. A. (1973) *Adv. Enzymol.* **38,** 317–371.
2. Krell, M. & Eisenberg, M. A. (1970) *J. Biol. Chem.* **245,** 6558–6566.
3. Huang, W., Jia, J., Gibson, K. J., Taylor, W. S., Rendina, A. R., Schneider, G. & Lindqvist, Y. (1995) *Biochemistry* **34,** 10985–10995.

4. Gibson, K. J., Lorimer, G. H., Rendina, A. R., Taylor, W. S., Cohen, G., Gatenby, A. A., Payne, W. G., Roe, C., Locket, B. A., Nudelman, A., *et al.* (1995) *Biochemistry* **34,** 10976–10984.
5. Alexeev, D., Baxter, R. L., Smekal, O. & Sawyer, L. (1995) *Structure* **3,** 1207–1215.
6. Baxter, L. R. & Baxter, H. C. (1994) *J. Chem. Soc. Commun.* 759–760.
7. Gibson, K. J. (1997) *Biochemistry* **36,** 8474–8478.
8. Huang, W., Lindqvist, Y., Schneider, G., Gibson, K. J., Flint, D. & Lorimer, G. (1994) *Structure* **2,** 407–414.
9. Alexeev, D., Baxter, R. L. & Sawyer, L. (1994) *Structure* **2,** 1061–1072.
10. Dreusicke, D., Karplus, P. A. & Schulz, G. (1988) *J. Mol. Biol.* **199,** 359–371.
11. Pai, E. F., Kabsch, W., Krengel, U., Holmes, K. C., John, J. & Wittinghofer, A. (1989) *Nature (London)* **341,** 209–214.
12. Murphy, J. E., Stec, B., Ma, L. & Kantrowitz, E. R. (1997) *Nat. Struct. Biol.* **4,** 618–622.
13. Lee, Y.-H., Olson, T. W., Ogata, C. M., Levitt, D. G., Banaszak, L. J. & Lange, A. J. (1997) *Nat. Struct. Biol.* **4,** 615–618.
14. Moréra, S., Chiadmi, M., LeBras, G., Lascu, I. & Janin, J. (1995) *Biochemistry* **34,** 11062–11070.
15. Otwinowski, Z. (1993) in *Proceeding of the CCP4 Study Weekend: Data Collection and Processing,* eds. Sawyer, L., Isaacs, N. & Bailey, S. (SERC Laboratory Daresbury, Warrington, UK), pp. 56–62.
16. Jones, T. A., Zou, J., Cowan, S. & Kjeldgaard, M. (1991) *Acta Crystallogr.* **A47,** 110–119.
17. Brunger, A. T. (1992) X-PLOR, *Version 3.1* (Yale Univ. Press, New Haven, CT).
18. Murshudov, G. N., Vagin, A. A. & Dodson, E. J. (1997) *Acta Crystallogr.* **D53,** 240–258.
19. Moffat, K. & Henderson, R. (1995) *Curr. Opin. Struct. Biol.* **5,** 656–663.
20. Pai, E. F., Krengel, U., Petsko, G. A., Goody, R. S., Kabsch, W. & Wittinghofer A. (1990) *EMBO J.* **9,** 2351–2359.
21. Knowles, J. R. (1980) *Annu. Rev. Biochem.* **49,** 877–919.
22. Herschlag, D. & Jencks, W. P. (1990) *Biochemistry* **29,** 5172–5179.
23. Yang, G., Sandalova, T., Lohman, K., Lindqvist. Y. & Rendina, A. (1997) *Biochemistry* **36,** 4751–4760.
24. Tali, L. W., Matte, A., Goldie, H. & Delbaere, L. T. J. (1997) *Nat. Struct. Biol.* **4,** 990–994.
25. Gupta, R. K., Oesterling, R. M. & Mildvan, A. S. (1976) *Biochemistry* **15,** 2881–2887.
26. Liaw, S. H. & Eisenberg, D. (1994) *Biochemistry* **33,** 675–681.